crystals

MDPI

Article

Structures, Electric Properties and STM Images of GeSe Monolayers Doped by Group IV–VI Atoms: A First-Principles Study

Hao Ni [1,2,†], Yonghong Hu [2,3,†], Guopeng Zhou [4], Caixia Mao [1,2], Zhiyuan Chen [2,3], Qingyong He [5,*] and Libing Qian [3,*]

1 School of Electronic and Information Engineering, Hubei University of Science and Technology, Xianning 437100, China
2 Hubei Key Laboratory of Radiation Chemistry and Functional Materials, Xianning 437100, China
3 School of Nuclear Technology and Chemistry & Biology, Hubei University of Science and Technology, Xianning 437100, China
4 Institute of Engineering Technology, Hubei University of Science and Technology, Xianning 437100, China
5 School of Physical Education, Hubei University of Science and Technology, Xianning 437100, China
* Correspondence: heqingyong@hbust.edu.cn (Q.H.); qianlb@hbust.edu.cn (L.Q.)
† These authors contributed equally to this work.

Abstract: Doping is an important method to modulate the physical and chemical properties of two-dimensional materials. By substitutional doping, different group IV–VI atoms are doped in GeSe monolayers to compose the doped models, of which the effects are investigated using first-principles calculations. The results show that local deformations of geometrical structure can be observed around the doping atoms. According to the analysis of the formation energy and the cohesive energy, all the doped models have a strongly bonded network, and GeSe_N possesses the most stable structure. Only the bandgap of Ge_As is direct, while those of other doped models are indirect. Thus, direct and indirect bandgaps are alternative by doping different atoms. The structural and electronic properties, especially for the bond lengths variation around doping atoms, are explained by the charge density difference. Finally, the scanning tunnel microscope images of the doped models are analyzed for further experimental investigations. Our work provides a stimulating account by atom doping which could trigger the developments and applications of new two-dimensional materials for manufacturing microelectronic and optoelectronic devices.

Keywords: GeSe monolayer; doping; first-principles calculation; electric property

check for updates

Citation: Ni, H.; Hu, Y.; Zhou, G.; Mao, C.; Chen, Z.; He, Q.; Qian, L. Structures, Electric Properties and STM Images of GeSe Monolayers Doped by Group IV–VI Atoms: A First-Principles Study. *Crystals* **2023**, *13*, 284. https://doi.org/10.3390/cryst13020284

Academic Editors: Younes Hanifehpour, Songang Peng, Yao Yao and Chaoyi Zhu

Received: 6 January 2023
Revised: 24 January 2023
Accepted: 2 February 2023
Published: 7 February 2023

Copyright: © 2023 by the authors. Licensee MDPI, Basel, Switzerland. This article is an open access article distributed under the terms and conditions of the Creative Commons Attribution (CC BY) license (https://creativecommons.org/licenses/by/4.0/).

1. Introduction

With some unique properties, two-dimensional (2D) materials, such as graphene [1], phosphorene [2], silicene [3] and germylene [4], etc., have drawn tremendous interest [5]. They are predicted to be promising materials to fabricate microelectronic, optoelectronic and energy devices in the next generation. Recently, many 2D mono-elemental semiconductors of group-III, -IV and -V elements have been predicted. Some of them, such as boron nitride [6], molybdenum disulfide [7], black phosphorus [8], etc., have been synthesized experimentally in some cases. For example, germanium monochalcogenides are found to be promising replacements for the lead chalcogenides in photovoltaic applications owing to their unique structural, electrical and optical properties [9]. According to previous studies, monolayer semiconductors, such as GeSe, GeS, SnS and SnSe, are sensitive and anisotropic with strain-tunable electronic properties. GeSe and SnSe both have direct bandgaps, 1.20 eV and 1.10 eV respectively [10–12]. The band gap of GeSe monolayer, which is the biggest of the four monolayer semiconductors above, can be tuned via strain engineering [13]. With some strain, the GeSe monolayer can be turned to be an indirect bandgap semiconductor. GeSe monolayers and double-layers are promising materials in the

field of ultra-thin-film photovoltaic applications [14–18]. With these outstanding features, GeSe has a bright prospect of future applications in ferroelectrics [19], thermoelectrics [20], photodetectors [21,22], etc.

Defects are often unavoidable while fabricating and processing the monolayer materials [23,24]. As we try to exfoliate the 2D monolayer from their substrates, some defects may be doped simultaneously. These defects are often undesirable atoms which we want to avoid. On the other hand, defects are vacancies, doping and topology, which may affect the mechanical, electronic and chemical properties of nanomaterials significantly. Thus, we can discover attractive applications by inducing defects to the semiconductor industry. Doping is considered to be an important method for changing the features of two-dimensional materials, including adding absorbed atoms and doping substitutional atoms [25]. Investigators often use doping along with substituting the sub-atoms to modulate the bandgap of monolayers for plenty of nanoscale applications [26–29]. For example, variable magnetic states could be induced by atom doping with transitional metal atoms [29]. Some properties of hydroxyapatites, such as thermal, morphological and structural parameters, can be modulated by yttrium-doping or Sm/Mg-doping [30,31]. As pristine GeSe monolayers are substitutionally doped by transition metals, they can be utilized as promising gas sensors to absorb small molecules [32].

In this paper, we take doped GeSe monolayers as the subject to investigate the structural and electronic features. Different doping atoms in group-IV, -V and -VI (Si, Pb, N, P, As, Sb, Bi, S, Se and Te) may lead to various properties of the doped system. The geometrical structure is firstly discussed for different doped models. The lattice parameter, bond angles and bond lengths around the doping atom are calculated. Then the stability of the doped system is analyzed via the calculation results of the formation energy, cohesive energy and bandgap. Electronic features, including the bandgap structure and the electron density, are investigated and compared with the pure GeSe monolayer, which is exhibited in our previous work [12]. Finally, the scanning tunnel microscope (STM) images of the doped GeSe monolayers are calculated to observe the atom arrangement related to the physical properties of the monolayer.

2. Computational Methods

All of the calculations are performed in the Cambridge Sequential Total Energy Package (CASTEP) [33] code based on the density functional theory (DFT) [34]. The package is a quantum mechanics program ab initio simulation tool including geometry optimization and energy calculation. The ultra-soft pseudo-potentials [35] are employed to approximate the interactions between ions and electrons. The generalized gradient approximation (GGA) of the Perdew-Burke-Ernzerhof (PBE) is adopted to describe the exchange and the correlation potential. The vacuum region is set to 20 Å, which is large enough to separate the interaction between the neighboring layers along the z-axis. All of the GeSe doped models are fully relaxed until the force per atom is less than 0.01 eV/Å. The energy deviation converges when it decreases to 5.0×10^{-6} eV/atom. The maximum stress deviation and displacement deviation are set to 0.02 GPa and 5.0×10^{-4} Å, respectively. According to the energy convergence test, a cutoff energy of 400 eV is set as the plane wave basis. The electronic self-consistent field (SCF) is set to 5.0×10^{-7} eV/atom to guarantee the accuracy of the calculations. The Brillouin zone in each original cell reciprocal is sampled by the Monkhorst-Pack mesh with $9 \times 3 \times 9$ k-points.

3. Results and Discussion

As a defect formation mechanism, doping can be divided into two categories. One is adding a new atom into a monolayer. The other is replacing an atom of the monolayer. Here, we choose the latter one to obtain the doped system.

3.1. Structural Properties

One of the Se atoms in the GeSe monolayer is replaced by Si, Pb, P, As, Sb, Bi, S or Te to generate the substitutional doped models. For example, the model doped by a Te atom is denoted as GeSe_Te in this paper. In total, there are 18 Se atoms in the doped GeSe monolayer that are used for the calculation and analysis of structural optimization and electrical properties. Thus the doping concentration is approximately 5.6%.

Figure 1 gives the doped model of GeSe_Te. One of the Se atoms in GeSe is chosen to be substituted by Te. There are five Te-Ge bonds, l_1, l_2, l_1',l_2' and l_3, denoted by white dotted arrows around the doping Te atom. The geometric structure of these five bonds seem to be the same as that of GeSe_Rh, the substitutional doped GeSe monolayer with a Rh atom [26]. The doped atoms in GeSe_Rh and GeSe_Te are quite different. The former is a Ge atom, while the latter in this work is a Se atom. However, intriguringly, the bond structures are almost the same. Among these bonds, l_2 and l_2' are two newly generated bonds after the substitution. The gray dotted arrows of l_0 and l_0' denote the two Ge-Se bonds existing in the pure GeSe monolayer. After doping, l_0 and l_0' disappear in GeSe_Te. This may be attributed to the enhanced interaction between the Te atom and its neighboring Ge atoms. Thus, l_0 and l_0' are broken by the stronger interaction. The bond angle of θ_1 is the in-plane angle between l_1 and l_2', while θ_2 is the out-of-plane bond angle of l_2 and l_3.

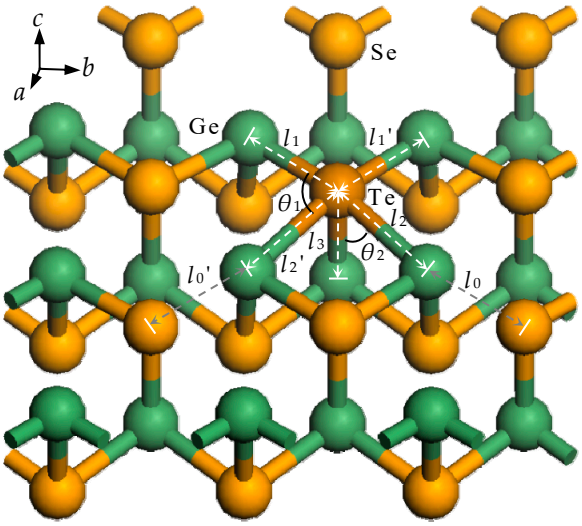

Figure 1. The perspective view of GeSe doped by a Te atom.

The parameters of the doped GeSe monolayers are shown in Table 1. In group-IV and -V, the lattice parameter of a increases with the size of the doping atom, while a decreases for group-VI. Considering the bond angle, it is obvious that the in-plane bond angle of θ_1 decreases with the size of the doping atom in each group. While doping a Sn, Pb or Bi atom, there are also five bonds between the doping atom and the neighboring Ge atoms. The measurement results exhibit the bond length equivalence of $l_1 = l_1'$ and $l_2 = l_2'$. In each group, it can be concluded that the bigger the doping atom, the easier it is to form five bonds. That is because the outer electrons are more active in the bigger atoms to generate bonds with the Ge atoms. It is quite different while doping other atoms of Table 1. There are only three bonds, l_1, l_1' and l_3, around the doped atoms of N, Si, S, P, As or Sb. There is $l_1 = l_1'$ while l_2, l_2' and θ_2 disappears. By doping the two largest atoms, GeSe_Pb and GeSe_Bi possess the longest bond length with their neighboring Ge atom. The bonds of l_1/l_1' and l_3 are approximately 2.9 Å and 3.1 Å respectively. The shortest bond lengths, 1.95 Å and 1.92 Å, appear in the GeSe_N monolayer. All of the bond-lengths increase with the size of the doping atoms in each group.

Table 1. The parameters of the doped GeSe monolayer with the group-IV, -V, and -VI atoms (Si, Sn, Pb, N, P, As, Sb, Bi, S, and Te): Lattice parameter (a), bond angles (θ_1 and θ_2), and bond lengths (l_1, l_2, l_1', l_2', and l_3) related with the doping atom.

Doping Atom Group	Doped Model	a (Å)	θ_1 (°)	θ_2 (°)	l_1 (Å) l_1' (Å)	l_2 (Å) l_2' (Å)
IV	GeSe_Si	11.69	95.3	-	2.62	-
	GeSe_Sn	11.73	89.6	84.2	2.49	2.93
	GeSe_Pb	11.84	70.8	68.9	2.90	3.05
V	GeSe_N	11.71	110.6	-	1.95	-
	GeSe_P	11.73	89.6	-	2.51	-
	GeSe_As	11.77	86.9	-	2.60	-
	GeSe_Sb	11.80	80.5	-	2.80	-
	GeSe_Bi	11.88	78.1	73.4	2.89	3.07
VI	GeSe_S	11.89	96.1	-	2.53	-
	GeSe_Te	11.73	89.6	84.2	2.49	2.93

The symbol of '-' denotes no bond or no angle.

The top view of the optimized geometrical structures for GeSe_Te is described in Figure 2a. Obviously, there are four bonds between the doping Te atom and its neighboring Ge atoms and no bond is found at l_0 and l_0'. Figure 2b gives the side view of GeSe_Te. The doping Te atom, behind the yellow Se atom labeled by the red dotted circle, is almost sheltered by the Se atom. Combining Figure 2a,b, the location of the doping Te atom is almost the same as that of the pure GeSe monolayer. We could also deduce that the bond length of l_3 is almost the same as that of the pure GeSe monolayer [12]. Part of the side views around the doping atoms for the other doped models are exhibited in Figure 2c. They are different from each other due to different doping atoms. Compared with the pure GeSe monolayer [12], the location of the doping atom is almost the same with the doped Se atom while doping with P, As, Sn or Te. The doping atom falls down while doping with N, S or Si. When the doping atom turns out to be Pb, Sb or Bi, the doping atom rises up with its neighboring Ge atom. Relatively, the obvious shift of the doping atom occurs with the substitution of N, Sb, Pb or Bi. This may be attributed to the larger atom size and the stronger metallicity between the two atoms of l_3 in Figure 1.

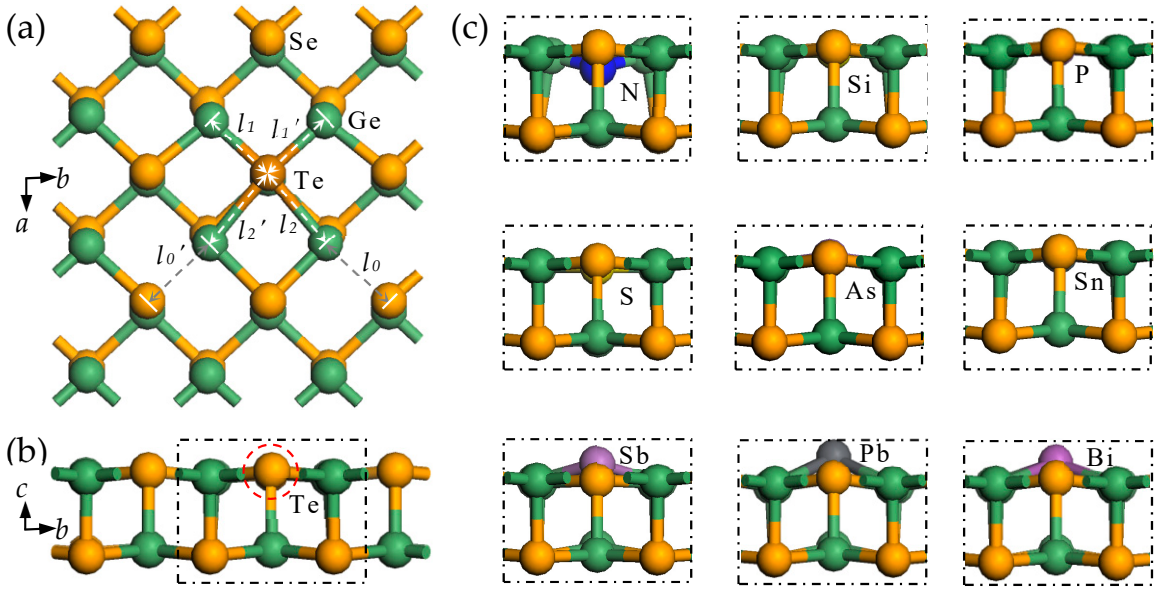

Figure 2. (**a**,**b**) Top and side view of GeSe monolayer doped by a Te atom. (**c**) A part of the side view of each doped GeSe model by one of group IV–VI atoms.

3.2. Stability

To evaluate the stability of the GeSe monolayer with different doping atoms, the cohesive energy E_{coh} and formation energy E_{form} are calculated to make the comparison. The formation energy of the doped system could be solved as [36]

$$E_{form} = E_{dope} - E_{pure} + \mu_{Se} - \mu_{dope}, \quad (1)$$

where μ_{Ge}, μ_{Se}, E_{dope} and E_{pure} denote the total energies of an isolated single Ge atom, an isolated Se atom, the doped GeSe monolayer, and the pure one, respectively. To further understand the structural stability, the cohesive energy per atom is calculated by

$$E_{coh} = \frac{n_{Ge}\mu_{Ge} + n_{Se}m_{Se} + n_{dope}m_{dope} - E_{dope}}{n}, \quad (2)$$

where $n = n_{Ge} + n_{Se} + n_{dope}$ is the total number of atoms in the doped system. There are 36 atoms in our doped GeSe model. One of the Se atoms is substituted by a group IV–VI atom. That is, we can obtain n = 36, n_{Ge} = 18, n_{Se} = 17, and n_{dope} = 1. According to Equations (1) and (2), the formation energy, cohesive energy and bandgap are calculated and these are shown in Figure 3.

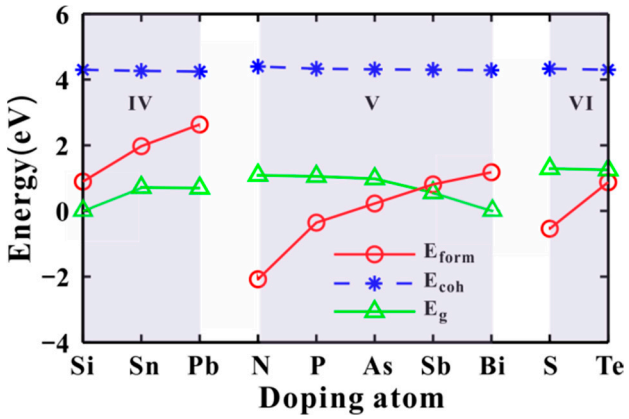

Figure 3. Formation energy (E_{form}), cohesive energy (E_{coh}) and bandgap (E_g) while doping different group IV–VI atoms into GeSe monolayers.

One can see that the values of E_{form} are quite different while doping 10 different atoms. The formation energies of GeSe_N, GeSe_P and GeSe_S are negative, while the others are positive. The negative formation energy indicates that it is easy to dope the atom in the GeSe monolayer while the positive value indicates difficulty. Therefore, it could be concluded that N, P, As, Sb, Bi and S are soluble in GeSe monolayer while the others are insoluble. While doping an N atom, the formation energy is -2.708 eV, which is the lowest of all. Thus, N-doping most easily forms a composite chalcogenide with the GeSe monolayer among the 10 atoms. On the contrary, doping a Sn atom to GeSe is the most difficult with a formation energy of 1.974 eV. Additionally, E_{form} is increasing monotonously with the size of the doping atom in each group.

In different doped models, the cohesive energy varies in the small range of 4.242 eV to 4.395 eV. For each group, E_{coh} is decreasing monotonously with the size of the doping atom. These common values of cohesive energy are very similar to those for other single-layer structures which are stable and are manufactured successfully [37]. Therefore, we can indicate that the proposed doped models all possess a strongly bonded network. Intriguingly, GeSe_N has the biggest value of cohesive energy and the smallest negative value of formation energy. It could be induced that GeSe_N possesses the most stable structure among the 10 doped models.

In our previous work, the bandgap of the pure GeSe monolayer is 1.20 eV [12]. While doping different atoms in each group, E_g is decreasing in this paper. The bandgap variation is the smallest while doping group-IV atoms. The bandgaps are around 1 eV while the doping atom is N, P or As. However, we obtained a bandgap of 0.263 eV by doping a Bi atom. This bandgap is so small that the system may sometimes exhibit some properties of a half-metal. Thus, the bandgap can be tuned into a wide range, from 0.263 eV to 1.084 eV while doping group-V atoms. As we move from dopant N to Bi, It is known to all that the semiconductor has a bandgap between the conduction band maxima (CBM) and the valence band maxima (VBM), while the CBM and VBM of the metal overlap with each other [38]. Thus, doping an atom with a stronger metallicity leads to a smaller bandgap. On the other hand, the size of the doping atom also increases from N to Bi. The larger the doping atom, the less attraction the nucleus has to its outmost electrons. It is easier for the outmost electrons to break away from the nucleus. If these outmost electrons are active enough, they could easily achieve an escape from the doping atom and shift away from VBM to CBM. Therefore, a smaller bandgap could be obtained with bigger doping atoms. This is in accordance with the performance with a strong metallicity of the doping atom, which is discussed above. By doping a S or a Te atom, we obtain the band gap of 1.254 or 1.293 eV, which is close to the bandgap of the pure GeSe monolayer [12]. Thus, the bandgap of the doped model can be tuned by doping atoms. Doping group-VI atoms could lead to a wider bandgap, owing to the stronger interaction between the Ge and the group-VI atoms. Compared with other former investigations [25,32], the bandgap varies monotonously with the atom size in a finite group.

3.3. Electronic Property

The bandgap structure and the partial density of states (PDOS) can be used to analyze the electronic properties systematically. The bandgap can be tuned by different strains which can cause the transfer between the direct semiconductor and the indirect semiconductor. Hence it has a bright future in the applications of electronic and optoelectronic devices. Figure 4 shows the site-projected band structures obtained using the PBE functional. Figure S1 gives some bandgap structures with the corresponding DOS. Most of the bandgaps lie within the range of visible light. Thus, these doped GeSe monolayers may be useful for optoelectric or solar energy conversion applications. Among the 10 doped models, only GeSe_As is a direct bandgap semiconductor, while others exhibit indirect bandgaps. The VBM tops of GeSe_S and GeSe_Te are at the formation energy of E_{form} = 0, which is the same as that of pure GeSe [12]. This may be attributed to the number of their outermost electrons. Se, S, and Te are all group-VI atoms. They all have four electrons in their outmost shell. Other VBM tops of the doped models are higher than E_{form} = 0. GeSe_As has the highest VBM of 0.788 eV, while GeSe_Sn has the lowest CBM of 0.913 eV. Compared with the pure model, the bandgaps of N, P, As, Sb, and Bi are less than that of pure GeSe [12] because of the decreasing CBM due to the p-type doping.

The PDOS (see Supplementary Materials Figure S2) shows that the VBMs of the doped models are dominated by the p orbitals of the Se and the doping atoms that are hybridized with s and p orbitals of the atoms, while the CBMs are dominated by the Ge p orbitals. Compared with the PDOS of the pure GeSe, the p orbital of the doping atom makes a notable contribution for the valence state of the doped model. Interestingly in GeSe_Te, there is an obvious peak at around -11 eV in the PDOS image of the s orbital of Te. This peak induces a new peak in the total DOS of GeSe_Te, which is different from those of other doped models.

To further understand the variations in the local geometry of the doped GeSe model, the charge density difference is calculated and shown in Figure 5. These figures are listed with an increase in the atom size. The red arrow and symbol are used to label the position of the doping atom in each figure. With different doping atoms, the optical spectra of the charge density difference are much different around the doping atoms. This is attributed to the local deformations induced by the presence of the doping atoms. The contour of the

charge density difference of the doping atom depends on the bond lengths. The doping N atom is near the top left/right Ge atom. We could deduce that there are two bonds between the doping N atom and the top left and top right Ge atoms. These two bonds are the shortest of all. Meanwhile, no bond exists between the N atom and its bottom left/right Ge atom (l_1 and l_1'), owing to the long distance. These deductions are in accord with the parameters of the bond lengths in Figure 2a and Table 1. As the size of the doping atom increases in Figure 5b–f, the doping atom moves gradually away from the top left/right Ge atom and towards the bottom left/right Ge atom. In Figure 5d,f, new bonds between the doping atom and its bottom left/right Ge atom (l_2 and l_2') arise by doping the Sn and Te atoms. Sn is the main element of group IVA, which has two valence states, positive bivalent and positive quadrivalent. Te has the same outermost electron number with the substituted Se atom and exhibits positive bivalent. Moreover, the atom sizes of Sn and Te are both large. Combing the valence states of positive bivalent and large atom size, the doping Sn and Te atoms generate four bonds with the neighboring four Ge atoms.

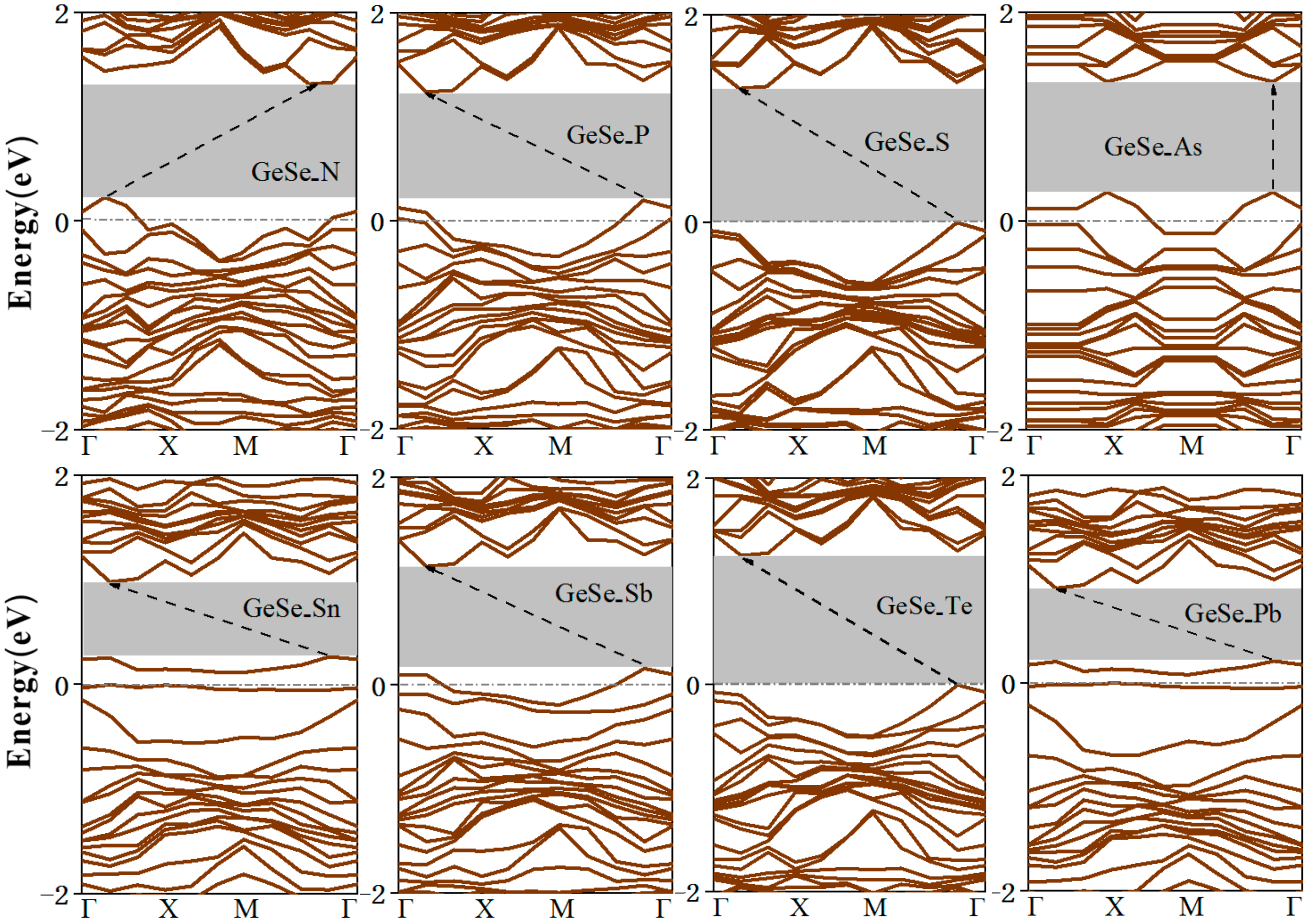

Figure 4. Electronic band structure of the doped model (GeSe_N, GeSe_P, GeSe_S, GeSe_As, GeSe_Sn, GeSe_Sb, GeSe_Te, and GeSe_Pb) for the most stable structures. The shaded region indicates the bandgap, and the dashed lines indicate the bandgap type.

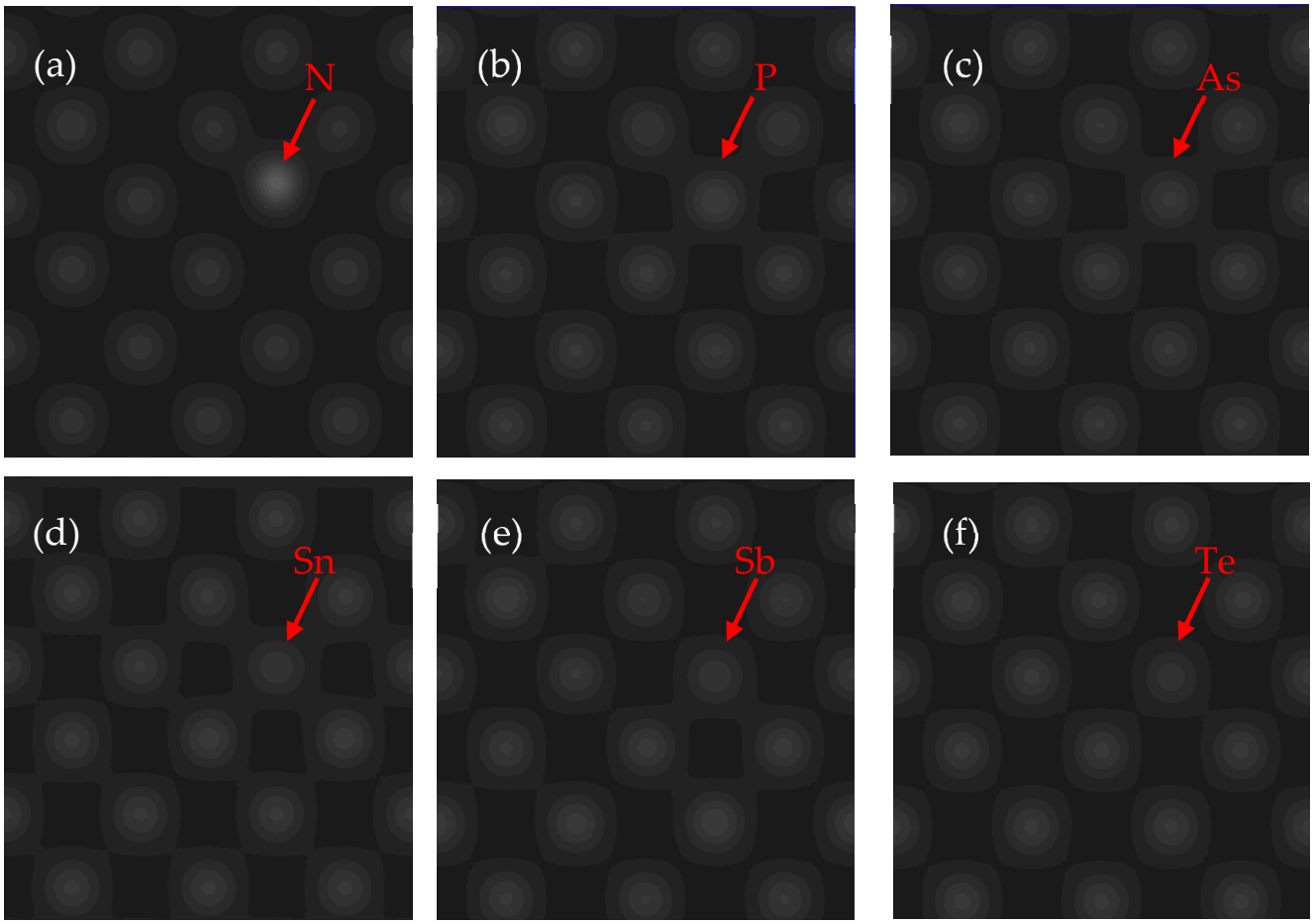

Figure 5. The slicing plane (parallel to the sheet of 2D material) of the charge density difference for the doped models of GeSe_N (**a**), GeSe_P (**b**), GeSe_As (**c**), GeSe_Sn (**d**), GeSe_Sb (**e**), and GeSe_Te (**f**).

3.4. STM Images

Some valuable differences among the scanning tunneling microscope (STM) images are found to promote future experiments; for instance, identifying the doping states. Under a positive bias of 2.0 V, the STM images in Figure 6 are simulated by the Tersoff-Hamann approximation, to better identify and to study the effects of the substantial doped GeSe monolayers. In Figure 6a, the atom N is a little darker and smaller than the Ge and Se atoms. The distance between the doping atom N and its neighbor atom Ge is the shortest, which is in accordance with the smallest radius of N and their shortest bond length in Table 1. The P, Sb, and Te atoms appear as white spots (shown in Figure 6b,e,f). The As atom tends to disguise as a Se atom. The difference between the As atom and the Se atom is very subtle (shown in Figure 6c). This may be attributed to their similar atom size. In the GeSe_Sn model (shown in Figure 6d), the brighter Sn and its two neighboring Ge atoms make up a "kidney". Though GeSe_Sn and GeSe_Te (shown in Figure 6f) possess almost the same geometric parameters, there is a striking contrast between their STM images. The STM images of GeSe_Sb (shown in Figure 6e) and GeSe_Te are similar to each other. However, the Sb atom is slightly brighter than the Te atom. That is because the Sb atom is not only higer than the initial Se atom in GeSe_Sb, but it is also higher than other doping atoms, according to Figure 2. Despite the location of the Te atom in Figure 6f is almost the same as that of the initial Se atom, the Te atom seems brighter owing to a larger radius of Te than those of Ge and Se. The crystal structures of doped systems with the atoms of N and Sn are easy to be identified through their STM images, while others are difficult.

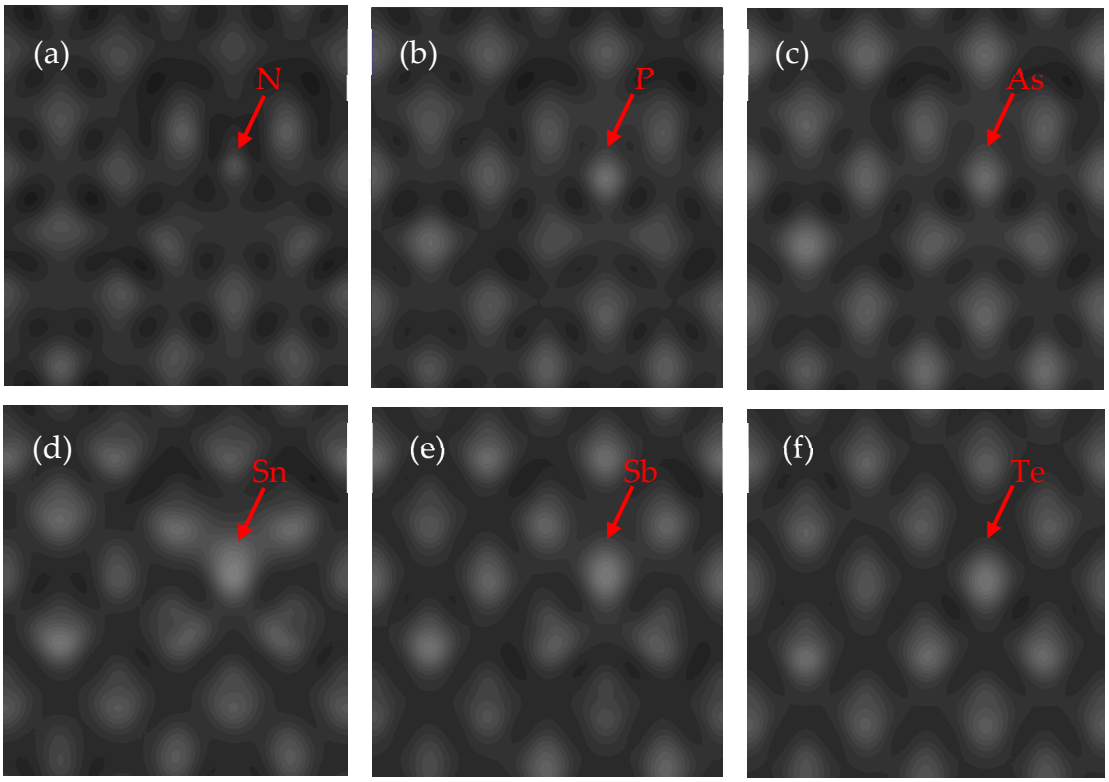

Figure 6. STM profiles of the doped models of GeSe_N (**a**), GeSe_P (**b**), GeSe_As (**c**), GeSe_Sn (**d**), GeSe_Sb (**e**), and GeSe_Te (**f**) under positive bias of 2 V.

4. Conclusions

In conclusion, we present a theoretical study on the effects of group IV–VI atom doping in monolayer GeSe. First-principles plane-wave calculations are performed systematically within DFT. According to the DFT results, the substitutional atom doping method leads to different local deformations of the doped system, especially for the part around the doping atom. In detail, the larger size of the doping atom attributes to longer bond lengths around the doping atoms in each group. The formation energy and the cohesive energy are both calculated to investigate the stability of the doped models. It has been found that doping N, S, and P are much easier, owing to the negative formation energy. Especially, the GeSe_N monolayer is the most stable among the 10 doped models. Bangap structure and DOS are provided to discuss the electric properties. Only GeSe_As has a direct bandgap, while other doped models possess indirect ones. The charge density difference further reveals that the bond lengths around the doping atoms are closely related to the size of doping atom. Moreover, the STM images are provided to recognize the substitutional doping method for further experiments. These systemic information exhibits the outstanding characteristics of the doped GeSe monolayer, which can pave the way for the development of low-dimensional microelectronics and optoelectronics in the upcoming days.

Supplementary Materials: The following supporting information can be downloaded at: https://www.mdpi.com/article/10.3390/cryst13020284/s1, Figure S1: Bandgap structure and the corresponding DOS of GeSe_N (a), GeSe_Pb (b), GeSe_Sn (c), and GeSe_Te (d); Figure S2: DOS and PDOS comparison of GeSe_N (a), pure GeSe (b), and GeSe_Te (c).

Author Contributions: Conceptualization, H.N. and Y.H.; methodology, H.N.; validation, Q.H.; formal analysis, Y.H.; investigation, Z.C. and Y.H.; resources, Z.C. and H.N.; data curation, C.M.; writing—original draft preparation, H.N.; writing—review and editing, H.N. and L.Q.; visualization, H.N.; supervision, Q.H.; project administration, Q.H.; funding acquisition, Y.H., G.Z. and L.Q. All authors have read and agreed to the submitted version of the manuscript.

Funding: This research was funded by the Scientific Research Project and Innovation Team of Hubei University of Science and Technology, China, grant number HKCXTD-001; the Key Research and Development Program of Hubei Province, China, grant number 2021BGD022; the Optical Valley Science and Technology Innovation Corridor Project of Hubei Province, China, grant number 2021BGE030, and the Scientific Research Foundation of Hubei University of Science and Technology, grant numbers BK202216, 2021ZX16, and 2021ZX02.

Data Availability Statement: The data presented in this study are available upon request.

Conflicts of Interest: The authors declare no conflict of interest.

References

1. Lee, C.; Wei, X.; Kysar, J.W.; Hone, J. Measurement of the elastic properties and intrinsic strength of monolayer graphene. *Science* **2008**, *321*, 385–388. [CrossRef]
2. Khandelwal, A.; Mani, K.; Karigerasi, M.H.; Lahiri, I. Phosphorene–the two-dimensional black phosphorous: Properties, synthesis and applications. *Mat. Sci. Eng. B-Adv.* **2017**, *221*, 17–34. [CrossRef]
3. Mu, W.C.; Riyadi, M.A.; Hamzah, A.; Alias, N.E.; Sultan, S.M.; Cheng, S.L.; Tan, M.L.P. Device performances analysis of p-type doped silicene-based field effect transistor using spice-compatible model. *PLoS ONE* **2022**, *17*, e0264483.
4. Lai, T.Y.; Fettinger, J.C.; Power, P.P. N-N double-bond cleavage and azobenzene rearrangement with C-C bond formation induced by a germylene. *Organometallics* **2022**, *41*, 1590–1594. [CrossRef]
5. Bhimanapati, G.R.; Lin, Z.; Meunier, V.; Jung, Y.; Robinson, J.A. Recent advances in two-dimensional materials beyond graphene. *ACS Nano* **2015**, *9*, 11509–11539. [CrossRef]
6. Golberg, D.; Bando, Y.; Huang, Y.; Terao, T.; Mitome, M.; Tang, C.; Zhi, C. Boron nitride nanotubes and nanosheets. *Acs Nano* **2010**, *4*, 2979. [CrossRef]
7. Tian, H.; Wu, X.; Zhang, K. Tailoring morphology and properties of tight utrafiltration membranes by two-dimensional molybdenum disulfide for performance improvement. *Membranes* **2022**, *12*, 1071. [CrossRef]
8. Gupta, S.N.; Singh, A.; Pal, K.; Chakraborti, B.; Muthu, D.; Waghmare, U.V.; Sood, A.K. Raman anomalies as signatures of pressure induced electronic topological and structural transitions in black phosphorus: Experiments and theory. *Phys. Rev. B* **2017**, *96*, 094104. [CrossRef]
9. Lv, X.; Wei, W.; Sun, Q.; Li, F.; Huang, B.; Dai, Y. Two-dimensional germanium monochalcogenides for photocatalytic water splitting with high carrier mobility. *Appl. Catal. B-Environ.* **2017**, *217*, 275–284. [CrossRef]
10. Hu, Y.; Zhang, S.; Sun, S.; Xie, M.; Cai, B.; Zeng, H. Gese monolayer semiconductor with tunable direct band gap and small carrier effective mass. *Appl. Phys. Lett.* **2015**, *107*, 122107. [CrossRef]
11. Lei, X.; Ming, Y.; Shi, J.W.; Yuan, P.F. Electronic and optical properties of the monolayer group-IV monochalcogenides MX(M = Ge, Sn; X = S, Se, Te). *Phys. Rev. B* **2017**, *95*, 235434.
12. Ni, H.; Li, M.; Hu, Y.; Mao, C.; Xue, L.; Zeng, H.; Yan, Z.; Wu, Y.; Zheng, C. Two-dimensional SnSe/GeSe van der Waals heterostructure with strain-tunable electronic and optical properties. *J. Phys. Chem. Solids* **2019**, *131*, 223–229. [CrossRef]
13. Li, Y.; Ma, K.; Fan, X.; Liu, F.; Xie, H. Enhancing thermoelectric properties of monolayer GeSe via strain-engineering: A first principles study. *Appl. Surf. Sci.* **2020**, *521*, 146256. [CrossRef]
14. Zhao, H.; Mao, Y.; Mao, X.; Shi, X.; Xu, C.; Wang, C.; Zhang, S.; Zhou, D. Band structure and photoelectric characterization of GeSe monolayers. *Adv. Funct. Mater.* **2018**, 1704855. [CrossRef]
15. Liu, S.; Mi, Y.; Xue, D.; Chen, Y.; He, C.; Liu, X.; Hu, J.; Wan, L. Investigation of physical and electronic properties of GeSe for photovoltaic applications. *Adv. Electron. Mater.* **2017**, *3*, 1700141. [CrossRef]
16. Zi, W.; Mu, F.; Lu, X.; Cao, Y.; Xiao, Z. Post-annealing treatment of a-GeSe thin films for photovoltaic application. *Sol. Energy* **2020**, *199*, 837–843. [CrossRef]
17. Li, Z.; Yan, H.J.; Liu, X.; Liu, S.; Feng, M.; Wang, X.; Yan, B.; Xue, D. Surface-defect states in photovoltaic absorber GeSe. *J. Phys. Chem. Lett.* **2021**, *12*, 10249–10254. [CrossRef] [PubMed]
18. Lv, X.; Wei, W.; Mu, C.; Huang, B.; Ying, D. Two-dimensional GeSe for high performance thin-film solar cells. *J. Mater. Chem. A* **2018**, *6*, 5032–5039. [CrossRef]
19. Chu, J.; Duan, C.; Xiang, P.; Wei, Z.; Guan, Z.; Zhao, Y.; Wang, X.; Zhong, N.; Deng, X.; Zheng, Y. Electric-field-induced room-temperature antiferroelectric-ferroelectric phase transition in van der Waals layered GeSe. *ACS Nano* **2022**, *16*, 1308–1317.
20. Yan, M.; Geng, H.; Jiang, P.; Bao, X. Glass-like electronic and thermal transport in crystalline cubic germanium selenide. *J. Energy Chem.* **2020**, *45*, 83–90. [CrossRef]
21. Ramasamy, P.; Kwak, D.; Lim, D.; Ra, H.; Lee, J. Solution synthesis of GeS and GeSe nanosheets for high-sensitivity photodetectors. *J. Mater. Chem. C* **2016**, *4*, 479. [CrossRef]
22. Afzal, A.; Iqbal, M.; Dastgeer, G.; Nazir, G.; Eom, J. Ultrafast and highly stable photodetectors based on p-GeSe/n-$ReSe_2$ heterostructures. *ACS Appl. Mater. Interfaces* **2021**, *13*, 47882–47894. [CrossRef]
23. Yang, Z.; Jiang, B.; Zhang, Z.; Wang, Z.; He, X.; Wan, D. The photovoltaic and photoconductive photodetector based on GeSe/2D semiconductor van der Waals heterostructure. *Appl. Phys. Lett.* **2020**, *116*, 141101. [CrossRef]

24. Hu, Y.; Shu, T.; Mao, C.; Xue, L.; Yan, Z.; Wu, Y. Arsenene and antimonene doped by group-VA atoms: First-principles studies of the geometric structures, electronic properties and STM images. *Physica B* **2019**, *553*, 195–201. [CrossRef]
25. Zhao, Y.; Li, X.; Li, H.; He, L. Modulation of the electronic properties and photocatalytic performance of black phase monolayer GeSe by noble metal doping. *New J. Chem.* **2021**, *45*, 15378. [CrossRef]
26. Wang, H.; Wang, Q.; Cheng, Y.; Li, K.; Yao, Y.; Zhang, Q.; Dong, C.; Wang, P.; Schwingenschlögl, U.; Yang, W.; et al. Doping monolayer graphene with single atom substitutions. *Nano Lett.* **2012**, *12*, 141–144. [CrossRef]
27. Zhang, K.; Feng, S.; Wang, J.; Azcatl, A.; Lu, N.; Addou, R.; Wang, N.; Zhou, C.; Lerach, J.; Bojan, V. Correction to manganese doping of monolayer MoS_2: The substrate is critical. *Nano Lett.* **2016**, *16*, 2125. [CrossRef]
28. Bafekry, A.; Faraji, M.; Hieu, N.N.; Khatibani, A.B.; Fadlallah, M.M.; Gogova, D.; Ghergherehchii, M. Tunable electronic properties of porous graphitic carbon nitride (C6N7) monolayer by atomic doping and embedding: A first-principle study. *Appl. Surf. Sci.* **2022**, *583*, 152270. [CrossRef]
29. Zhang, H.; Wang, N.; Wang, S.; Zhang, Y. Effect of doping 3D transition metal (Fe, Co, and Ni) on the electronic, magnetic and optical properties of pentagonal ZnO_2 monolayer. *Physica E* **2020**, *117*, 113806. [CrossRef]
30. Ahmed, L.O.; Bulut, N.; Kebiroglu, H.; Alkhedher, M.; Ates, T.; Koytepe, S.; Ates, B.; Kaygili, O.; Din, E.M.T.E. Effects of Yttrium Doping on Erbium-Based Hydroxyapatites: Theoretical and Experimental Study. *Materials* **2022**, *15*, 7211. [CrossRef]
31. Hssain, A.H.; Bulut, N.; Ates, T.; Koytepe, S.; Kuruçay, A.; Kebiroglu, H.; Kaygili, O. The experimental and theoretical investigation of Sm/Mg co-doped hydroxyapatites. *Chem. Phys. Lett.* **2022**, *800*, 139677. [CrossRef]
32. Zhang, T.; Pan, W.; Zhang, Z.; Qi, N.; Chen, Z. Theoretical study of small molecules adsorption on pristine and transition metal doped GeSe monolayer for gas sensing application. *Langmuir* **2022**, *38*, 1287–1295. [CrossRef] [PubMed]
33. Vanderbilt, D. Soft self-consistent pseudopotentials in a generalized eigenvalue formalism. *Phys. Rev. B* **1990**, *41*, 7892–7895. [CrossRef] [PubMed]
34. Paul, J.T.; Singh, A.K.; Dong, Z.; Zhuang, H.L.; Hennig, R.G. Corrigendum: Computational methods for 2D materials: Discovery, property characterization, and application design. *J. Phys-Condens Matter.* **2020**, *32*, 159501. [CrossRef]
35. Ceperley, D.M.; Alder, B.J. Ground state of the electron gas by a stochastic method. *Phys. Rev. Lett.* **1980**, *45*, 566–569. [CrossRef]
36. Hu, Y.; Zhang, S. Influences of Stone-Wales defects on the structure, stability and electronic properties of antimonene: A first principle study. *Physica B* **2016**, *503*, 126–129. [CrossRef]
37. Xu, C.; Zhu, M.; Zhang, J.; Wang, W.; Yan, Y. New two-dimensional allotrope of single layer IV-V semiconductor XBi (X = Si, Ge, Sn). *Comp. Mater. Sci.* **2018**, *150*, 314–320. [CrossRef]
38. Usman, M.; Mendiratta, S.; Lu, K.L. Semiconductor metal–organic frameworks: Future low-bandgap materials. *Adv. Mater.* **2016**, *29*, 1605071. [CrossRef]

Disclaimer/Publisher's Note: The statements, opinions and data contained in all publications are solely those of the individual author(s) and contributor(s) and not of MDPI and/or the editor(s). MDPI and/or the editor(s) disclaim responsibility for any injury to people or property resulting from any ideas, methods, instructions or products referred to in the content.